Pharm Res (2018) 35: 97
https://doi.org/10.1007/s11095-018-2382-9

RESEARCH PAPER

Transferrin-Modified Vitamin-E/Lipid Based Polymeric Micelles for Improved Tumor Targeting and Anticancer Effect of Curcumin

Omkara Swami Muddineti [1] • Preeti Kumari [1] • Balaram Ghosh [1] • Swati Biswas [1]

Received: 9 November 2017 / Accepted: 4 March 2018 / Published online: 14 March 2018

ABSTRACT

Purpose Transferrin receptor (TfR) is up-regulated in various malignant tumors not only to meet the iron requirement, but also to increase the cell survival via participation in various cellular signaling pathways. Here we explored transferrin as ligand for Poly(ethylene Glycol) (PEG)-ylated vitamin-E/lipid (PE) core micelles (VPM).

Methods Transferrin modified polymer was synthesized and drug loaded micelles were evaluated in 2D Hela and HepG2 cancer cells for cellular uptake and cytotoxicity and in 3D Hela spheroids for growth inhibition, uptake and penetration studies.

Results Targeted (Tf-VPM) and non-targeted (VPM) micelles showed mean hydrodynamic diameter of 114.2 ± 0.64 nm and 117.4 ± 0.72 nm and zeta potential was -22.8 ± 0.62 and -14.8 ± 1.74 mV, respectively. Cellular uptake study indicated that the Tf-CVPM were taken up by cancer cells (Hela and HepG2) with higher efficiency. Enhanced cytotoxicity was demonstrated for Tf-VPM compared to CVPM. Marked spheroid growth inhibition following treatment with Tf-CVPM was observed compared to the treatment with non-targeted CVPM.

Conclusions The developed transferrin-modified micelles have improved ability to solubilize the loaded drugs and could actively target solid tumors by its interaction with over-expressed transferrin receptors. Therefore, the nano-micelles could be further explored for its potential utilization in cancer therapy.

KEY WORDS active targeting · curcumin · micelles · transferrin · vitamin E

ABBREVIATIONS

CUR	Curcumin
C-VPM	Curcumin loaded VPM
DMEM	Dulbecco's modified Eagle's media
DOPE	Dioleoyl phosphatidylethanolamine
FBS	Heat-inactivated fetal bovine serum
FC	Free curcumin
h	Hour
Hela	Human cervical carcinoma cells
HepG2	Human hepatic carcinoma cells
MEM	Minimuim essential medium
MTT	Dimethylthiazol-2-yl)-2,5-di-phenyltetrazolium bromide
PEG-PE	Polyethylene glycol-phosphatidyl ethanolamine
pNP-PEG-PE	p-Nitrophenylcarbony-PEG-PE
PPM	PEG-PE based micelles
Tf	Transferrin
Tf-CVPM	Curcumin loaded Tf-VPM
Tf-PP	Transferrin modified PEG-PE
Tf-VP	Transferrin modified Vitamin E based polymer
Tf-VPM	Transferrin modified vitamin E based micelles
VPM	Vitamin E based micelles

INTRODUCTION

Cancer is one of the most life-threatening diseases, which caused death of 8.2 million people and around 14.1 million people were newly diagnosed with cancer globally in 2012. Even though many approaches have prevailed in the recent

Electronic supplementary material The online version of this article (https://doi.org/10.1007/s11095-018-2382-9) contains supplementary material, which is available to authorized users.

✉ Swati Biswas
swati.biswas@hyderabad.bits-pilani.ac.in

[1] Department of Pharmacy
Birla Institute of Technology & Science-Pilani, Hyderabad Campus
Jawahar Nagar, Shameerpet, Hyderabad, Telangana 500078, India

years for the treatment of cancer, however, cure for cancer still remains elusive (1). Various chemotherapeutic agents, including paclitaxel, docetaxel, doxorubicin, camptothecin, gemcitabin and cisplatin have been used in the clinic as conventional chemotherapy, either alone or in combination to kill cancer cells for recession of the growth of tumor (2). However, conventional chemotherapy suffers several drawbacks, including non-specific toxicity and non-tumor targetability, and development of multiple drug resistance (MDR) (3,4). Cancer cells over-express various efflux transporters on cell surface, including P-glycoprotein, multiple drug resistance protein, and breast cancer resistance protein. The transporters efflux the drug out, thus, reduce the intracellular drug concentration to sub-optimum level. Therefore, emergence of MDR limits the therapeutic efficacy of conventional chemotherapy (5–7).

Nano-sized drug delivery systems (DDS) offer advantages over conventional chemotherapy for cancer treatment. Various nanoparticles, including liposomes, polymeric micelles, lipid and inorganic nanoparticles have been utilized for the delivery of chemotherapeutic agents in cancer. In addition to imparting stability and improving the biopharmaceutical properties of the loaded drug, long circulating nanocarriers eventually accumulate to the tumor site via Enhanced Permeability and Retention (EPR) effect, thus promoting tumor-targeted accumulation of the loaded cargo (2,8,9). Nanocarriers can be surface modified to impart multifunctionality to the drug delivery system. For instance, (i) Poly(ethylene glycol) (PEG) can be conjugated on the surface for long circulation, the DDS-forming polymer can be suitably designed for stable assembly and better loading of the therapeutic cargo, and the polymer can be degraded in response to external stimuli for faster on site drug release (10,11).

D-alpha-tocopheryl succinate (α-TOS) is a vitamin E derivative, which has been conjugated previously to polymers to prepare various DDS (12–14). α-TOS has demonstrated antiproliferating, and apoptosis-inducing effect in various cancer cell lines. Tocopherol polyethylene glycol succinate (TPGS), a nonionic, amphiphilic compound inhibited cellular drug resistance by inhibiting drug efflux transporter, P-gp by exerting ATPase inhibition (14). Considering the therapeutic benefit of α-TOS in cancer therapy, various polymers have been conjugated to α-TOS and utilized in drug delivery application for therapy-resistant tumors. For example, Li *et al.*, have developed poly (L-lactide)-vitamin E TPGS (PLA-TPGS) based micelles and delivered doxorubicin to MCF-7/ADR cells successfully. The results confirmed that higher efficacy of the formulation was due to the combination of inhibition of P-gp efflux and enhanced accumulation of doxorubicin into the nucleus in drug-resistant MCF-7/ADR cells (15).

Surface-modification of nanocarriers with various targeting ligands to improve the tumor directed intracellular delivery of nanocarriers by recognizing cell surface-over-expressed receptors have been widely utilized to improve therapeutic efficacy (16–18). Transferrin, a glycoprotein of molecular weight ~80 KDa is a vital iron transport protein in serum, which maintains the iron homeostasis in biological fluids and controls the growth of cells (19). Due to the higher rate of proliferation and subsequent iron demand, cancer cells over-express transferrin receptors (100 fold higher) than the normal cells (17,20–22). Hence, transferrin has been explored as a surface-modifying ligand for nanocarriers to achieve active tumor targeting (19,23–25). In our earlier work, we have developed an α-TOS/lipid-based co-polymeric micellar system (VPM) that conjugated α-TOS and dioleoyl-phosphatidylethanolamine (DOPE) with PEG via the lysine amino acid linker (26). The newly developed micellar system displayed lower critical micelles concentration, higher drug loading and encapsulation efficiency compared to plain PEG-PE polymeric micelles. VPM exhibited multiple drug resistance inhibitory potential on resistant murine melanoma cells. The passive targeting of model hydrophobic anticancer drug, curcumin (CUR)-loaded VPM demonstrated improved cytotoxicity compared to PEG-PE micelles (PPM) towards cancer cells *in vitro* and *in vivo*. In this work, we have developed an actively tumor-targeted VPM, which anchored transferrin on the surface for recognition by the over-expressed transferrin receptors on the cancer cells. The polymeric micelles (Tf-VPM) were loaded with anticancer drug, CUR, physico-chemically characterized, and evaluated for their targetability, and cytotoxicity in Tf-over-expressing Human cervical carcinoma (Hela) and human hepatic carcinoma (HepG2) cells. Finally, the tumor-inhibitory potential of Tf-VPM has been evaluated in 3D-HeLa spheroidal model.

MATERIALS AND METHODS

Materials

1,2-dipalmitoyl- *sn*-glycero-3- phosphoethanolamine-N-(lissamine rhodamine B sulfonyl) (Rh–PE) and 2-dioleoyl-*sn*-glycero-3-phosphoethanolamine-*N*-(glutaryl) (DOPE-Glutaryl) were purchased from Avanti Polar Lipids (Alabaster, AL); pNP-PEG_{3400}-pNP was purchased from LaysanBio (Arab,AL). Transferrin, Fmoc-Lys(boc)-OH, *N*-(3-Dimethylaminopropyl)-*N'*-ethylcarbodiimide hydrochloride (EDC) and N-hydroxysuccinimide (NHS), Polyethylene glycol amine phospatidyl ethanolamine (PEG_{5k}-PE), anhydrous chloroform, α-tocopheryl succinate, fluorescence-free glycerol-based mounting medium (fluoromount-G), CUR, human transferrin (recombinant expressed in rice) and pyrene were procured from Sigma Aldrich Chemicals (Bangalore, India). Dialysis membranes (1kD, 2kD, 12-14kD, 100 kD) were obtained from Spectrum Laboratories, Inc. (California, USA). Methoxy PEG (5 K) amine hydrochloride (mPEG-Amine.HCl) was purchased from Jenkem technologies,

(Texas, USA).1. Trypan blue and 3-(4, 5-dimethylthiazol-2-yl)-2, 5-di-phenyltetrazolium bromide (MTT) were procured from Himedia Laboratories (Mumbai, India). Organic solvents and chemicals procured commercially were of analytical grade or higher.

Human cervical carcinoma (HeLa) and human hepatic carcinoma (HepG2) cells were procured from the National center for cell science (NCCS, Pune, India). Agarose, Accutase™, 3-(4, 5-dimethylthiazol-2-yl)-2,5-di-phenyltetrazolium bromide (MTT) and trypan blue solution, minimuim essential medium (MEM), Dulbecco's modified Eagle's media (DMEM), heat-inactivated fetal bovine serum (FBS) and penicillin/ streptomycin were purchased from Himedia Laboratories (Mumbai, India). Other solvents and chemicals were of analytical grade, and were purchased from Sigma Aldrich (Bangalore, India). Cell lines were grown in DMEM supplemented with 10% FBS, 100 IU/mL of penicillin, streptomycin at 37 °C and 5% CO_2.

Synthesis of Vitamin E Based Co-Polymer

Vitamin E based co-polymer was synthesized as reported earlier, using acid-amine coupling reactions as shown in Fig. S1 (26). The intermediate and final polymers were purified by dialyzing against DI water for 48 h and lyophilized to get fluffy powders (27). Polymers were characterized by using ^{1}H NMR and GPC as reported in the earlier report.

Synthesis of pNP-PEG3400-PE Polymer

pNP-PEG3400-PE was synthesized according to the previously reported procedure as shown in Fig. 1 (21). Briefly, into the solution of pNP-PEG_{3400}-pNP in anhydrous chloroform and triethylamine (TEA) was added DOPE (mol ratio for pNP-PEG_{3400}-pNP: DOPE = 3:1). The reaction mixture was stirred overnight at room temperature, and evaporated to dryness by rotary evaporator to remove chloroform. The product was separated from unreacted PEG by using a Sepharose™ (CL4B) column using 0.1 N HCl in water as the eluent. The eluted fractions were spotted on silica coated plate to run TLC followed by staining the TLC plates with Dragondorff's reagent for the detection of pure pNP-PEG_{3400}-PE spot. First few fractions were pooled together, and lyophilized to obtain pure product. The lyophilized material was reconstituted with chloroform as 10 mg/mL stock solution and stored at −80°C.

Transferrin Modification of the Synthesized Polymer (Tf-VP)

Targeted micelles (Tf-VPM) were prepared by modification of pre-formed VPM micelles with Tf-PEG_{3400}-PE (Tf-PP) using post insertion method (28). Tf-PP was prepared as follows: Into the solution of pNP-PEG-PE

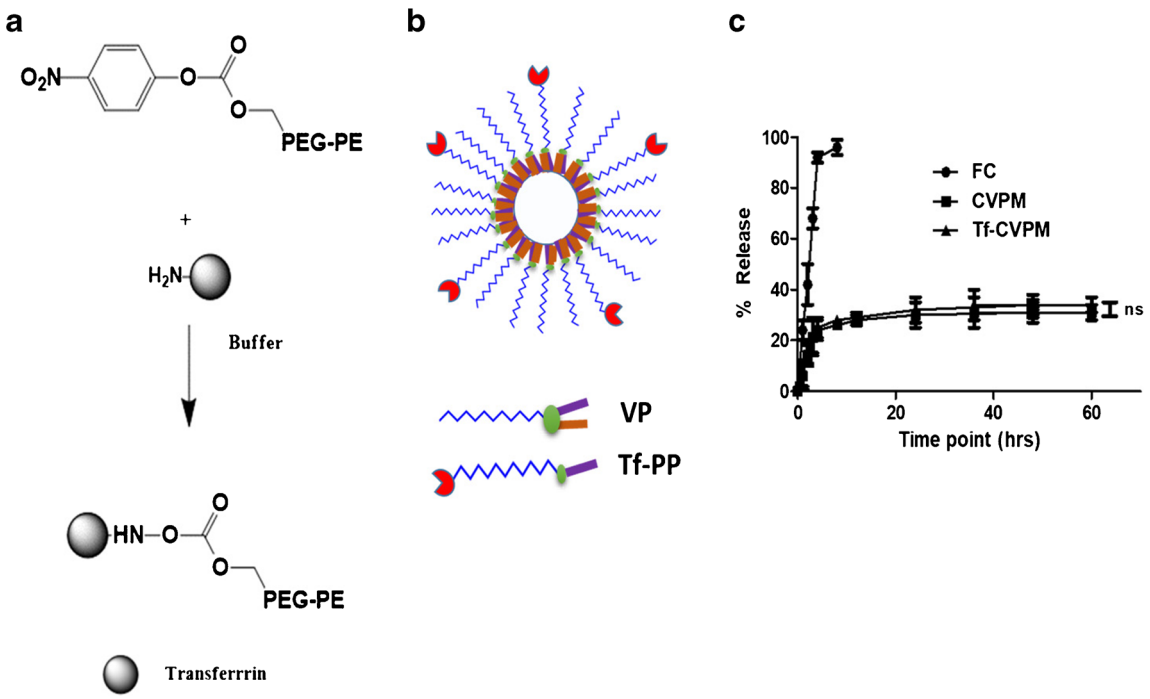

Fig. 1 Modification of PEG-PE polymer using transferrin (Tf) to prepare Tf-PEG-PE, (**b**). Schematic representation of Tf modified VPM and (**c**). *in vitro* drug release studies (pH 7.4) using dialysis method.

(0.11 mg) in citrate buffer, pH 5.0 was added transferrin (6.35 mg) in PBS, pH 8.5. The solution was stirred overnight at 4°C under nitrogen atmosphere. The activated acid group, pNP reacted readily with the free amine group in Tf to form Tf-PP. After overnight incubation, the solution of Tf-PP (1.86 mL of 2.5% *w/v* solution in HEPES, pH 7.4) was mixed with pre-formed VPM or CVPM micelles (1.0 mL of 2.5% w/v solution in HEPES, pH 7.4) and stirred overnight at 4°C for post-insertion of the Tf-PP in VPM. Unreacted Tf was removed by performing extensive dialysis for 24 h by using cellulose ester membrane of MWCO. 100 KDa against HEPES buffer, pH 7.4. BCA protein assay was performed to determine the protein content in the Tf-VPM solution by using the calibration curve of bovine serum albumin as the standard protein (Fig. S4).

Characterization of Micelles

Size, Zeta Potential and Morphological Analysis

The particle size and zeta potential were measured by dynamic light scattering using zetasizer (Nano ZS 90, Malvern Instruments Ltd., UK). Freshly prepared micelles were diluted appropriately and all measurements were taken at 25°C after equilibrating the instrument for 10 min. The data was measured in triplicates. Further, micelles were observed under transmission electron microscopy (TEM, JEM-1200EX, JEOL, Tokyo, Japan). For TEM analysis, samples were added onto a copper grid coated with a carbon membrane. The grid was allowed to dry before visualization.

Drug Release Profile of CVPM and Tf-CVPM

CVPM, Tf-CVPM and free CUR solution (at CUR concentration 1 mg/mL) were transferred into the dialysis bags (MWCO 12–14 k Da) and were immersed in 0.1 M PBS (pH 7.4 and pH 5.5) containing 0.1% (*w/v*) Tween 80 at 37°C under shaking at 90 rpm. (29) Samples (0.1 mL) were collected at predetermined time points from outer phase and replaced by the same volume of release medium. The amount of drug released into the media was quantified by analyzing the collected samples for CUR absorbance by using UV-Visible spectroscopy at the wavelength of 420 nm. Experiments were done in triplicates and % release was expressed as mean ± SD.

Entrapment Efficiency (EE) and Drug Loading (DL)

Drug loaded micelles were diluted by 80% (*v*/v) ethanol for micellar disassembly. The encapsulated drugs were analyzed by using UV-Visible spectrophotometer at a wavelength of 420 nm to determine the CUR concentration (30,31). EE and DL of CUR loaded micelles were calculated by using the following equations:

$$\text{EE (\%)} = (\text{Weight of CUR loaded/Weight of CUR taken}) \times 100\% \quad (1)$$

$$\text{DL (\%)} = (\text{Weight of CUR loaded/Weight of drug loaded micelles}) \times 100\% \quad (2)$$

Stability of the Micelles

The stability of the drug loaded micelles was studied during storage at 2–8°C by monitoring the particle size using zeta sizer. The drug content of the stored sample was estimated by using UV-Visible spectroscopy (at λmax 420 nm). Further, stability at physiological conditions was estimated by incubating Tf-CVPM in MEM medium supplemented with 10% fetal bovine serum at 37°C for 24 h prior to analyzing the particle size. Stability of the micelles was also analyzed at pH 7.4 and 5.5 for 72 h.

Cellular Uptake of CUR Loaded Micelles

Fluorescence Microscopy

HeLa and HepG2 cells (5×10^4 cells/well) were seeded in 12-well tissue culture plates supplemented with circular cover slips and set aside for overnight. The Following day, CVPM, Tf-CVPM, and FC were added into the wells at concentrations of 50 and 100 μg/mL (in serum free medium) and incubated for 1 and 4 h. In few wells, excess free transferrin (100 μM) was added and incubated for 30 min prior to the addition of Tf-CVPM. The process is adopted to saturate the Tf-receptors that mediates cellular targeting and internalization of the Tf-CVPM. Similarly chlorpromazine (30 μM) was used as clathrin receptor inhibitor to study the internalization mechanism. Incubation medium was discarded, and the cells were washed with PBS followed by addition of DAPI solution (5 μg/mL) for 5 min. Further, cells were washed thoroughly with PBS to remove DAPI. Cells were fixed by the treatment with 4% *w/v* paraformaldehyde for 10 min at room temperature. Then coverslips were mounted on microscopic glass slide using fluoromount G and visualized under a fluorescence microscope (Leica DMi8 inverted, Germany) using DAPI and FITC filters at 40X resolution. All images were captured at corresponding filter and analyzed by image *J* software version 1.6.0.

Flow Cytometry

Quantification of the cellular association of CUR was determined by using flow cytometer (Amnis Flowsight, United States). HeLa and HepG2 cells (4×10^5 cells/well) were seeded in 6-well tissue culture plates and incubated for overnight.

The following day, cells were treated with CVPM and Tf-CVPM at CUR concentration of 50 and 100 μg/mL for 1 and 4 h. The medium was discarded after completion of the incubation periods. Cells were washed, trypsinized, and transferred to 15 mL centrifuge tubes and subjected to centrifugation at 1000 rpm for 5 min at 4°C to obtain cell pellets. Pellets were suspended in cold PBS (200 μl) to perform flow cytometry (argon laser λexc at 488 nm). Fluorescence of CUR from the gated cells (10,000 cells) was collected to generate single parameter histogram. The data was collected in triplicates and analyzed using Ideas Analysis Software (Version 6.0).

Cytotoxicity Study

Cytotoxicity study was performed using MTT assay with HeLa and HepG2 cells lines. Briefly, HeLa and HepG2 cells were seeded separately in 96-well plates using 100 μl of growth medium at a density of 5000 cells/well, one day prior to adding CUR loaded formulations. The concentrations were maintained in the range of 0–50 μg/mL for 6 and 24 h as reported earlier (10,28). The media were discarded at respective incubation periods (either 6 h or 24 h). The cells undergone 6 h incubation were incubated further in drug-free complete media for 24 h before performing the MTT assay. For MTT assay, cells were incubated using serum free media containing aqueous MTT solution (50 μL; 5 mg/mL) for 4 h. Then, the solution was discarded and dimethyl sulfoxide (150 μl) was added to all wells to solubilize insoluble formazan crystals by shaking for 30 min at room temperature. Cell viability was estimated by measuring absorbance at 590 nm (620 nm as reference) using Spectramax™ multiplate reader (Molecular devices, US). % Cell viability was expressed using the following equation.

$$\%\text{cell viability} = Abs_{sample}/Abs_{control} \times 100$$

where, Abs_{sample} was the absorbance of the cells treated with FC, CVPM, Tf-VPM, Tf-CVPM, while $Abs_{control}$ was the absorbance of untreated cells. The results were reported as the mean absorbance ± SD for three replicates.

Tumor Spheroid Studies

Preparation of Cancer Cell Spheroid

HeLa cells were grown to spheroids of size of about 400–500 μm diameter in 96-well plates or 8 well plates following liquid overlay method as previously described (28). Briefly, MEM with 1.5% of agarose was used as base and 10,000 cells were seeded to grow as tumor spheroid. After formation of solid spheroid mass, plates were centrifuged for 15 min at 1500 RCF to form the compact spheroids. Size of the spheroids was assessed using Leica DMi8 inverted microscope.

Uptake in Spheroids

Spheroidal uptake of CUR following treatment with FC and Tf-CVPM at CUR concentration of 25 μM was assessed using fluorescence microscopy following incubation period of 1 h and 4 h. Following incubation, the treated spheroids were taken out from the 8-well plates to 1.5 mL centrifuge tubes, disassociated by incubating with Accutase™ (200 μL) for 20 min and then made into cell suspensions. These cell suspensions were made free from excess CUR by washing them with sterile PBS, pH 7.4. Cells suspension was suspended in 500 μl of PBS prior to analyzing the cells by using flow cytometer (Amnis Flowsight, United States) in triplicates.

Penetration Efficacy

Depth of penetration of CUR in spheroids was measured by using confocal microscope (Leica DMi8 confocal microscope, Germany). HeLa spheroids were developed in 8 well glass chamber slides (SPL Life science, Korea) and were incubated with FC and Tf-CVPM at CUR concentration 25 μM for 1 h and 4 h. Fluorescence intensity of CUR was tracked by using appropriate laser (λexc at 420 nm and λemi at 450–650). Z-stack images were captured in confocal microscope by using 10× objective at 10 μm interval of thickness from the top surface towards the tumor spheroid equatorial plane. Micrographs were analyzed by using *Image J* software.

Inhibition Study

HeLa spheroids were grown in 96 well tissue culture plates for 4 days. Following selection on the basis of uniform size and integrity, spheroids were incubated with Tf-CVPM and FC at CUR concentration of 25 μM for 9 days. Growth of the spheroids was monitored using inverted fluorescence microscopy (Leica DMi8 inverted fluorescence microscope) at predetermined time periods (0, 3, 6 and 9 days) as described earlier (32,33). Inhibition of spheroid growth was measured using the following formula: $V = (\pi \times d_{max} \times d_{min})/6$, where d_{max} is the maximum diameter and d_{min} is the minimum diameter of each spheroid (34).

RESULTS

Synthesis of Tf-VPM

Synthesis of the α-tocopherol-conjugated VPM was reported elsewhere following the scheme represented in Fig. S1 (26). The p-nitrophenyl (pNP) group conjugated acid-functionalized PEG-PE reacted readily with transferrin to form Tf-PP (Fig. 1). Unreacted Tf was separated by performing extensive dialysis. The % of Tf incorporation

was ~63% as determined by bicinchoninic acid (BCA) protein assay. The calibration curve using BCA as standard has been represented in Fig. S2. 2.5 mol% of Tf-PEG-PE was added to VPM and CVPM to form Tf-VPM and Tf-CVPM respectively by incubating them for overnight. Finally the targeted micelles were collected and used for further analysis.

Characterization of Tf-VPM

Both targeted (Tf-CVPM). and non-targeted micelles (CVPM) were loaded with CUR. Particle size and encapsulation efficiency was found to be 144.8 ± 0.94 nm and 98% respectively for Tf-CVPM. Loading of CUR was 14.34 ± 0.14 and 14.75 ± 0.16 for CVPM and Tf-VPM, respectively as shown in Table I. CVPM and Tf-CVPM did not show any significant difference in particle size and zeta potential which implies that modification with Tf did not alter the physicochemical properties. Transmission electronic microscopic image was provided in Fig. S3. For both Tf-CVPM and CVPM, the hydrodynamic diameter ranged from 140 to 145 nm, while the zeta potential of the non-targeted and Tf- targeted micelles was −22.8 ± 0.62 and −14.8 ± 1.74 mV, respectively. The characterization data ind-6icated that the addition of the Tf targeting moiety did +6not significantly alter the micellar physico-chemical properties. *In vitro* release studies at both +pH 7.4 and 5.5 showed faster release for FC (less than 4 h) and sustained release of curcumin for micellar formulations in 48 h (Fig. 1c and Fig. S4).

Stability of the Micelles

Tf-VPM demonstrated no significant change in particle size, PDI at 4°C for 3 months. The drug-loaded, Tf-CVPM did not show reduction in drug content indicating that both, blank and CUR-loaded micelles were stable at storage condition. Further, stability of the micelles were assessed in complete cell culture medium (MEM) to mimic physiological condition during systemic circulation. PDI was slightly increased, however, significant difference in the particle size before and after incubation was not observed indicating suitability of the Tf-CVPM for systemic administration as shown in Table II. Similarly stability studies pH 7.4 and 5.5 did not show significant difference in the particle size as shown in Table S1.

Cellular Uptake Studies

To assess the uptake of CUR by cancer cells, HeLa and HepG2 cells were treated with CVPM and Tf-CVPM for the time period of 1 and 4 h. As stated earlier, the transferrin receptors of cells in few wells, which received Tf-CVPM were saturated by pre-incubating the cells with excess transferrin at concentration 200 μg/mL for 1 h, and denoted with Tf-CVPM in the Fig. 2. CVPM and Tf-CVPM showed higher green fluorescence of CUR at 4 h compared to 1 h post treatment confirming the time dependent cellular association in both the cell lines. In saturation experiment using free Tf, Tf-CVPM displayed faint signal of CUR indicating the reduced cellular uptake into the cells. Similar studies were performed in both the cell lines using flow cytometer to quantitatively compare the cell-associated CUR-fluorescence following various treatments. The fluorescence intensity of HeLa cells at 4 h treated with CVPM and Tf-CVPM is much stronger (Geo means of fluorescence 24,895 ± 25, and 16,452 ± 32 for Tf-CVPM and CVPM, respectively) than 1 h treatment with the same formulations (Geo mean 16,453 ± 23, and 6524 ± 12, for Tf- CVPM and CVPM, respectively) (Figs. 2b and 3b). The Flow cytometry data in both the cell lines confirmed the significance in the difference of cellular association of transferrin modified and unmodified micelles. In competitive experiments, cell-associated CUR-fluorescence was decreased in Tf-pre-treated cells compared to Tf-untreated cells. To further elucidate the internalization mechanism of Tf-CVPM, cells were pre-incubated with endocytosis-pathway inhibitor, chlorpromazine. A marked decrease in the CUR-fluorescence resulting from the pre-saturation was observed (Fig. 3c).

Cytotoxicity

Cytotoxic potential of various treatments, including Tf-CVPM, CVPM, Tf-VPM, VPM and FC was determined in HeLa and HepG2 cells. Targeted nano-micelles, Tf-CVPM exhibited highest cytotoxicity at all tested CUR concentrations (0–50 μg/mL) compared to CVPM, Tf-VPM, VPM and FC after 24 h for both the cell lines as shown in Fig. 4. The superior cytotoxic effect of Tf-CVPM was observed in HepG2 cells compared to HeLa cells in both the time point studies (6 h followed by 24 h drug-free incubation and 24 h

Table I Characterization of Blank and Drug Loaded Micelles

Micelles	Particle size (nm) (Mean ± SD)	PDI	Zeta potential (mV) (Mean ± SD)	DL (Mean ± SD)	EE (Mean ± SD)
VPM	114.2 ± 0.64	0.214 ± 0.024	−28.8 ± 0.94	…	…
Tf-VPM	117.4 ± 0.72	0.192 ± 0.024	−16.2 ± 0.84	…	…
CVPM	141.6 ± 0.34	0.272 ± 0.038	−22.8 ± 0.62	14.75 ± 0.16	98.2 ± 0.46
Tf –CVPM	144.8 ± 0.94	0.276 ± 0.064	−14.8 ± 1.74	14.34 ± 0.14	98.6 ± 0.38

Table II Stability of Micelles in MEM Complete Medium

Micelles	Before incubation		After incubation	
	Particle size (nm) (Mean ± SD)	PDI	Particle size (nm) (Mean ± SD)	PDI
VPM	114.2 ± 0.64	0.214 ± 0.024	115.6 ± 0.46	0.238 ± 0.034
Tf-VPM	117.4 ± 0.72	0.192 ± 0.024	116.8 ± 0.48	0.216 ± 0.046
CVPM	141.6 ± 0.34	0.272 ± 0.038	143.6 ± 0.58	0.294 ± 0.042
Tf -CVPM	144.8 ± 0.94	0.276 ± 0.064	143.8 ± 0.94	0.286 ± 0.062

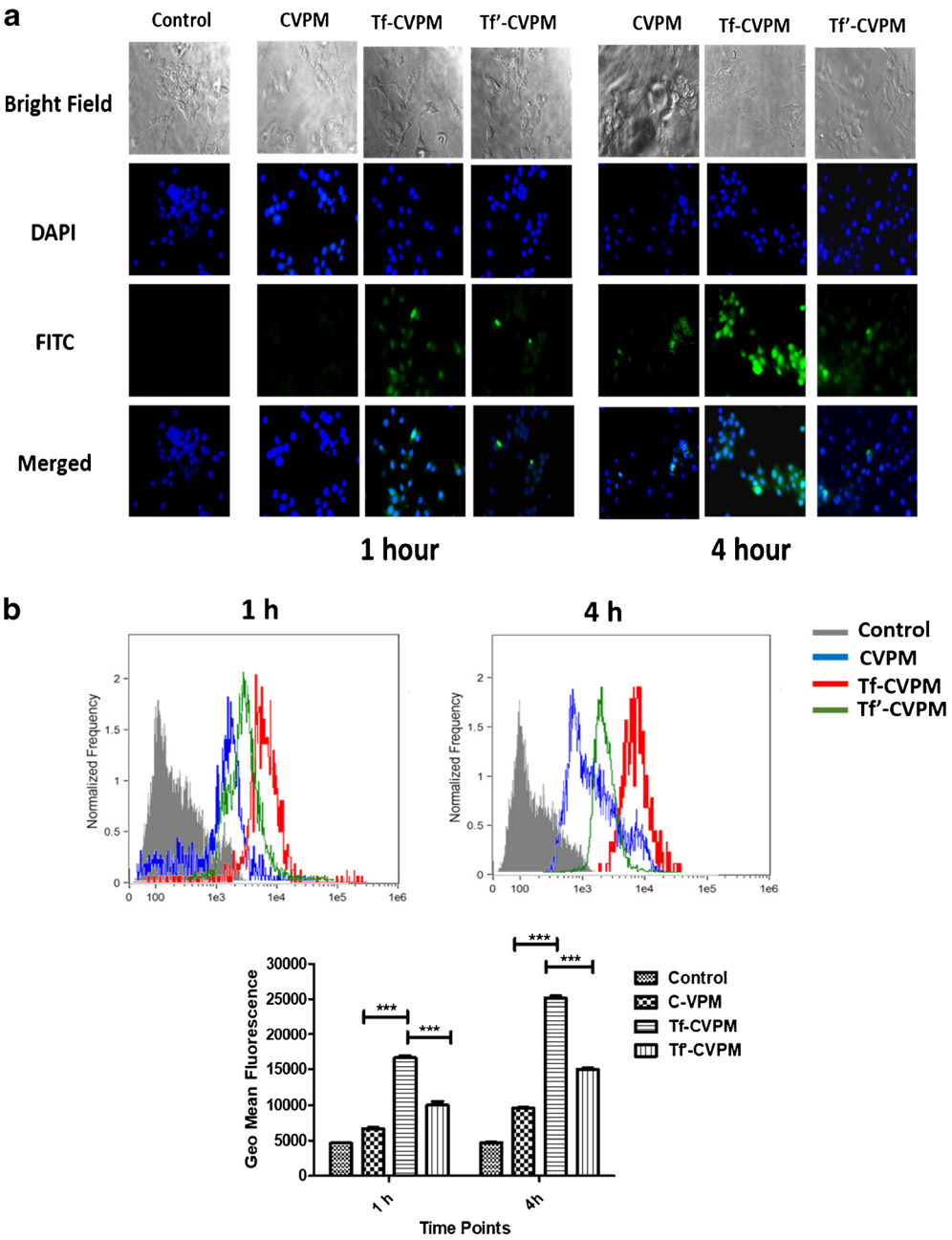

Fig. 2 Assessment of cellular uptake of CUR in HeLa cells. (**a**) Fluorescence micrograph of HeLa cells treated with VPM and Tf-CVPM for 1 h and 4 h (Tf'-CVPM in the Figure label represents the images of cells treated with free Tf before treatment with Tf-CVPM), (**b**) Flow cytometry data of HeLa cells treated with CVPM, Tf-CVPM at CUR concentration of 50 and 100 μg/mL for 1 and 4 h. Cell nuclei were stained with DAPI (blue). The cells were visualized in dual channels using DAPI (ex/em 350/460), and FITC filter (ex/em 495/520). Scale bar indicates 50 μm. Geo mean fluorescence data are represented as mean ± SD, averaged from three separate experiments. The significance of difference between the means was analyzed by Student's t-test, ***$p < 0.001$.

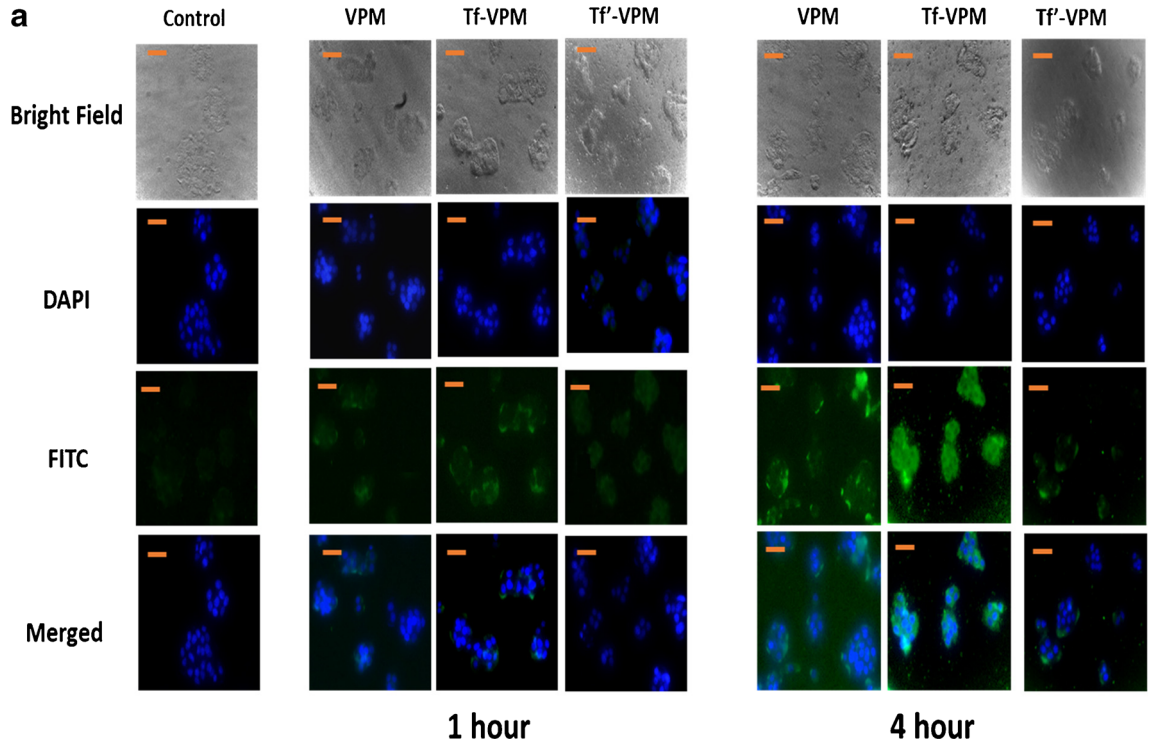

Fig. 3 Assessment of cellular uptake of CUR in HeLa and HepG2 cells. (**a**) Fluorescence micrograph of HepG2 cells treated with VPM and Tf-CVPM for 1 h and 4 h (Tf'-CVPM represents the images of cells treated with free Tf before treatment with Tf-CVPM), (**b**) Flow cytometry data of HeLa cells treated with CVPM, Tf-CVPM at CUR concentration of 50 and 100 μg/mL for 1 and 4 h. (**c**) Assessment of the mechanism of internalization of Tf-CVPM by using clathrin-mediated endocytosis inhibitor, chlorpromazine. Cell nuclei were stained with DAPI (blue). The cells were visualized in dual channels using DAPI (ex/em 350/460), and FITC filter (ex/em 495/520). Scale bar indicates 50 μm. Geo mean fluorescence data are represented as mean ± SD, averaged from three separate experiments. The significance of difference between the means was analyzed by Student's t-test, ***$p < 0.001$.

treatment) compared to other treatments. Tf-VPM caused significantly higher cytotoxicity compared to VPM at both the time points of 6 h and 24 h in both the cell lines.

Spheroid Studies

Spheroid Uptake

Spheroid uptake of CUR was analyzed by using flow cytometry at two different time points of 1 and 4 h (Fig. 5a). Geometric mean fluorescence of CUR was significantly higher for cells treated for 4 h compared to 1 h confirming the time dependent cellular uptake of the CUR in the spheroids. Similarly, geo mean fluorescence of spheroidal cells treated with Tf-CVPM was significantly higher compared to CVPM at both the time points of 1 h and 4 h (Geo mean fluorescence of 925 ± 18 and 648 ± 13 at 1 h, and 1651 ± 28 and 1125 ± 24 at 4 h for Tf-CVPM and CVPM, respectively).

Penetration Studies

Tumor penetration efficiency of various formulations was analyzed using confocal microscopy by assessing CUR fluorescence at different focal planes in the spheroid (Z slices) represented in Fig. 5a. The distribution of CVPM and Tf-CVPM in spheroids was analyzed by visualizing the CUR fluorescence after 1 h and 4 h incubation by confocal microscopy (Fig. 5b). Tf-CVPM showed higher fluorescence intensity of CUR in the middle stacks indicating the ability of the micellar formulation to penetrate deeper tumor mass compared to non-targeted CVPM.

Growth Inhibition

Spheroid growth inhibition was assessed by treating the cells with Tf-CVPM and CVPM at CUR concentration of 25 µM for 9 days. The data is represented in Fig. 5c. Spheroids were observed every day for change in morphology and images were captured using Leica DM8 inverted microscope (bright field). The treated spheroids were photographed (bright field) to measure their diameter (converted to volume) and to assess any morphological changes in the spheroids. Significant increase in spheroidal diameter was observed in control spheroids (~543 µm and ~1215 µm on day 0 and day 9, respectively). On day 9, the Tf-CVPM treated spheroid showed suppression in growth as indicated by the reduced spheroidal diameter of about ~598 µm compared to the diameter of control spheroids (~1215 µm). Untargeted CVPM had significant spheroidal growth inhibitory effect (spheroidal diameter

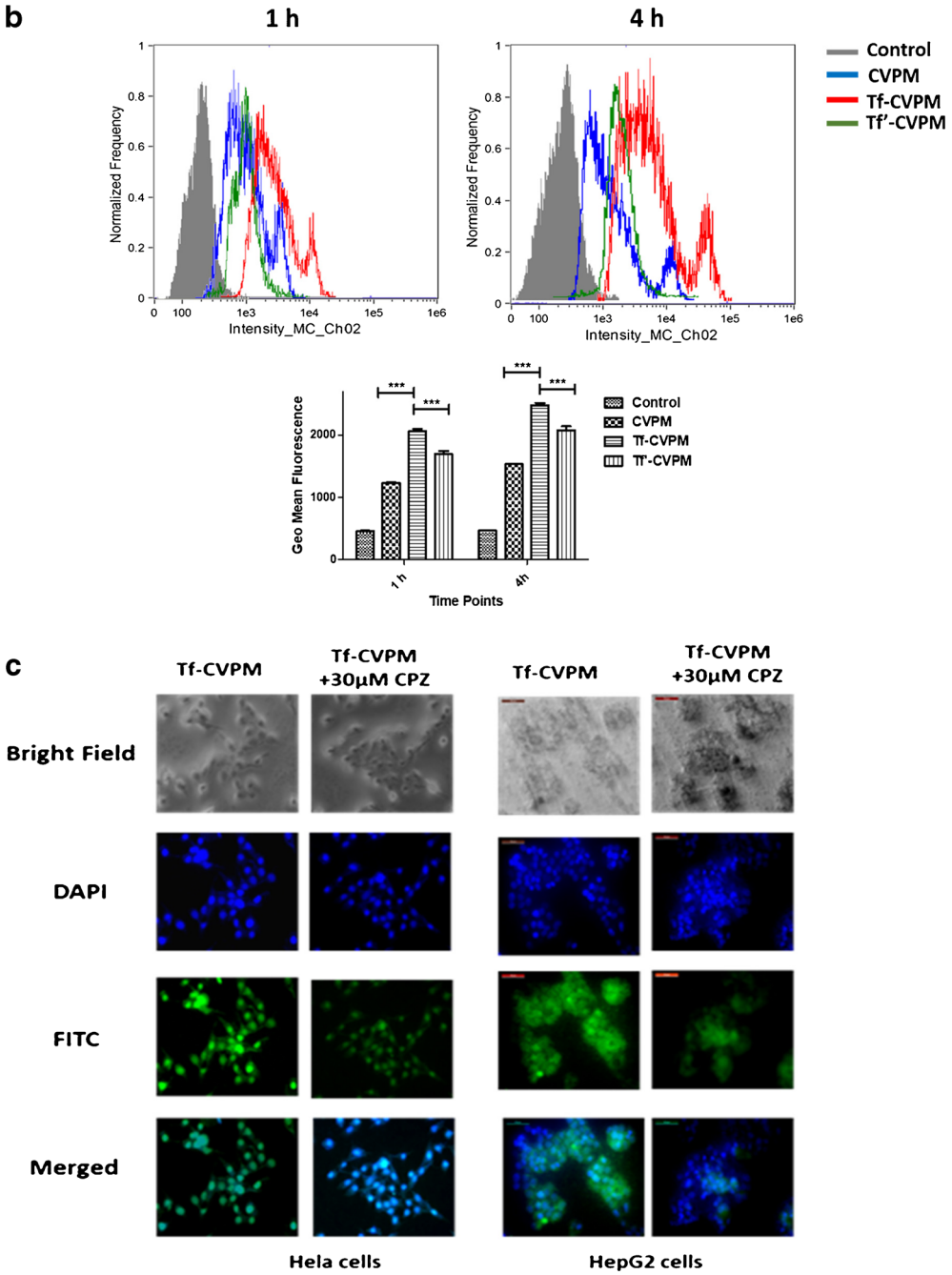

Fig. 3 (continued)

of ~900 μm on day 9 compared to control spheroidal diameter of ~1215 μm), however, a marked reduction of spheroidal size was evident following Tf-CVPM treatment.

DISCUSSION

The self-assembled amphiphilic polymer having DOPE and α-tocopherol as hydrophobic core and PEG 5 k as hydrophilic corona linked together via an amino acid Lysine (27) was synthesized in our previous work, and the developed polymeric micelles (VPM) demonstrated improved drug loading ability and therapeutic efficacy with the potential to reverse the multiple drug resistance compared to plain PEG-PE micelles (26,27). Further, in this study, VPM has been surface-modified with a tumor homing ligand, transferrin (Tf) to explore whether Tf-modified VPM (Tf-VPM) could stably hold and deliver the therapeutic cargo, CUR in higher concentration to the cancer cells leading to improved anticancer activity compared

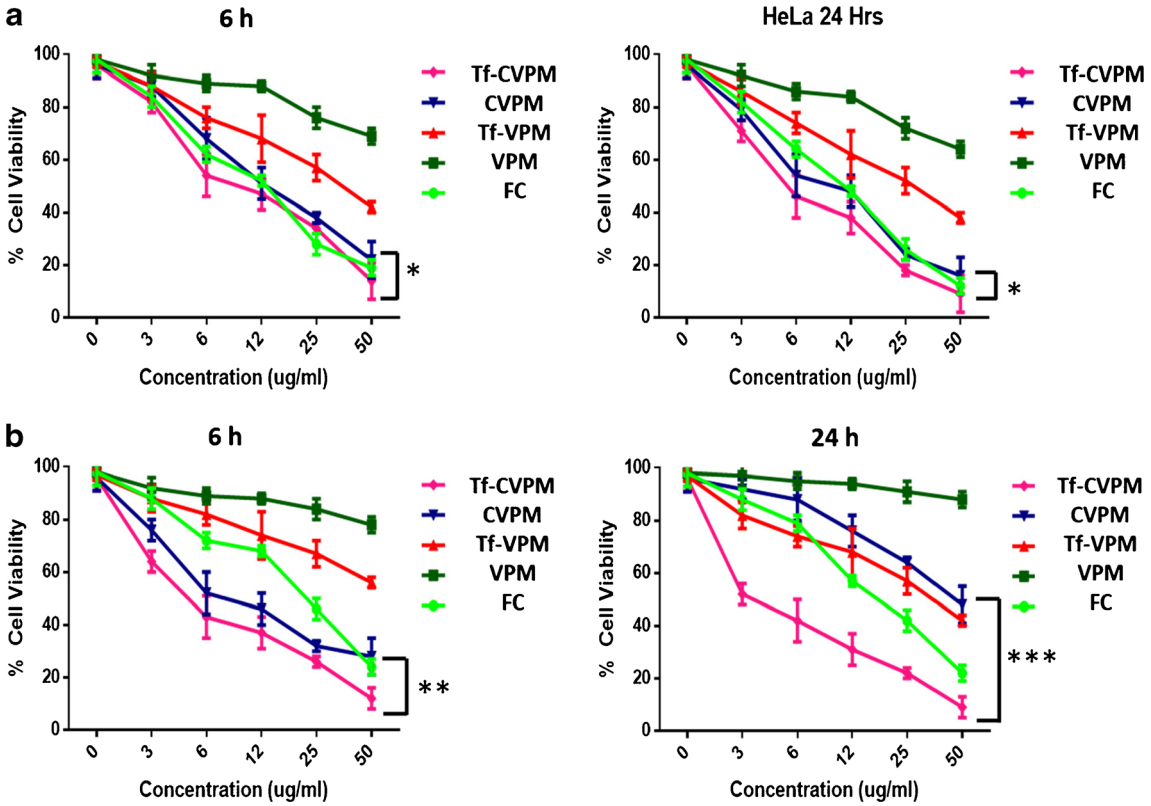

Fig. 4 Cytotoxic potential of the treatments in HeLa (**a**) and HepG2 cells (**b**). Cells were treated with FC, VPM, Tf-VPM, CVPM and Tf-CVPM at CUR concentration of 0–50 μg/mL for 6 h (followed by 24 h drug-free incubation) and 24 h. The significance of difference between the mean was analyzed by Student's t-test, ***, ** and * indicates $p < 0.001$, 0.01 and 0.05 respectively.

to unmodified VPM. Initially, Tf was conjugated to PEG-PE by using an activated acid-functionalized PEG-PE, pNP-PEG-PE (Fig. 1). The reactive pNP group in the synthesized pNP-PEG-PE was rapidly conjugated with amino groups of Tf under basic conditions (pH > 8) and dialyzed against cellulose ester membrane (MWCO. 100 KDa) to remove unconjugated Tf or the polymer. The Tf-conjugation efficiency was ~64% after purification as calculated from BCA protein assay. The newly synthesized, Tf-PEG-PE (2.5 mol%) was used to prepare blank or CUR-loaded formulation using post insertion technique as discussed in Materials and Methods section. Surface modification of micelles with Tf did not affect the particle size, DL, EE of the formulation. The particles were spherical as visualized by transmission electron microscopy (Fig. S3). Comparison data of various physico-chemical characteristics of the micellar nano-formulations are represented in Table I. The data clearly indicated that modification of surface using 2.5 mol% Tf did not affect the physico-chemical properties of CVPM (10). *In vitro* drug release studies indicated that the loaded CUR was released in sustained manner for both the Tf-CVPM and CVPM (at pH 7.4 and 5.5). However, the free drug CUR dissolved in propylene glycol showed complete released initial 4 h. Stability studies did not show any significant deviation in the particle size and PDI of the Tf-CVPM compared to CVPM on storage and on incubation with complete media (Table II). Similar results were obtained when micelles were incubated with at different condition pH 5.5 and pH 7.4 (Table S1). Based on the stability data, it was inferred that the developed Tf-CVPM can be stored at 4°C for minimum 3 months, and could safely be administered systemically. It can be envisioned that Tf-VPM would protect the loaded cargo for the period, from the systemic administration to delivery to the tumor, which usually could happen in less than 24 h.

Cellular uptake studies of indicated both concentration and time dependent uptake of the formulations (CVPM, and Tf-CVPM) as per qualitative (fluorescence images) and quantitative analysis (Geo mean fluorescence) as shown in Figs. 2 and 3. It was also observed that theTf modified, Tf-CVPM showed higher cellular association compared to CVPM. Saturation of Tf-receptors by pre-incubation of cells with excess Tf indicated that the Tf receptors were involved in endocytosis of the Tf-CVPM micelles. Pre-incubation blocked the Tf receptors by competitive inhibition of the uptake of Tf-CVPM micelles. The study proved the mechanism of internalization of Tf-CVPM, which was primarily by interacting with Tf-receptors via surface-anchored Tf. As Tf receptors are over-expressed on the cell surface of both the cell lines, HeLa and HepG2, Tf-

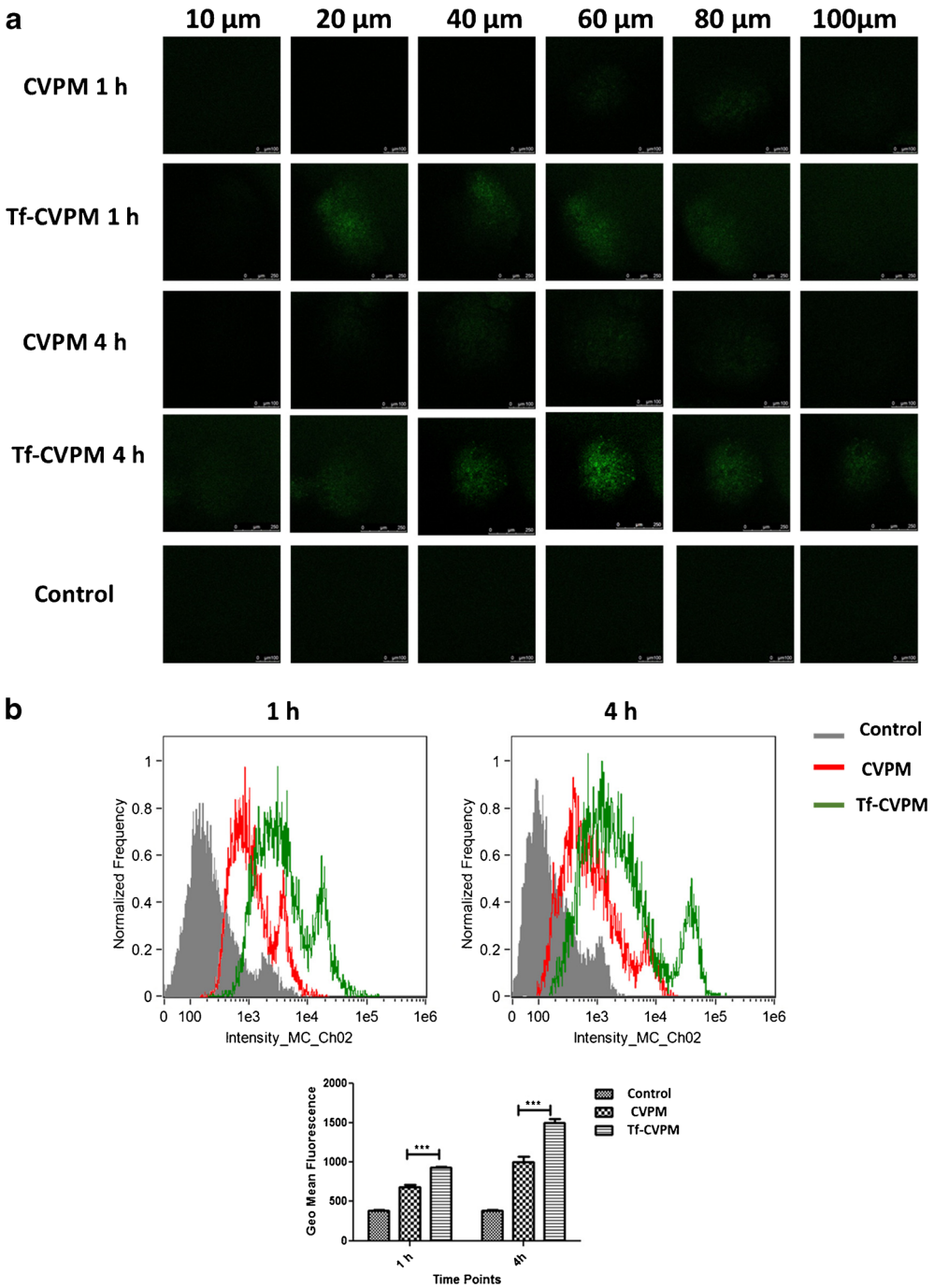

Fig. 5 Assessment of HeLa spheroidal uptake of CUR and growth inhibition. (**a**). Penetration of Tf-CVPM, and CVPM throughout HeLa spheroids. The distribution of CUR was analyzed by confocal microscopy using Z-stack imaging at 20 μm intervals from surface to inside the spheroids. (**b**). Overall spheroidal uptake of CUR via treatment by CVPM, and Tf-CVPM at both 1 h and 4 h time points analyzed by flow cytometry. Geo mean fluorescence data are mean ± SD, averaged from three separate experiments. (**c**). Phase-contrast images of spheroids treated with Tf-CVPM, CVPM (25 μM of CUR) for 9 days. Changes in the diameter of spheroids subjected to different treatments has been graphically represented in (**d**). The significance of difference between the means was analyzed by Student's t-test, ***, ** and * indicates $p < 0.001$, 0.01 and 0.05 respectively.

CVPM showed marked receptor mediated active targeting as measured by assessing loaded CUR fluorescence. Further investigation on the mechanism of internalization of demonstrated that the Tf-CVPM was internalized by clathrin-mediated endocytosis (Fig. 3c). As Tf receptors (TfR) are largely concentrated within the clathrin-coated pits, the result supported the mechanism of internalization of Tf-CVPM via clathrin-mediated endocytosis as reported earlier (35–37).

Cytotoxicity studies have proven the apoptosis inducing activity of blank micelles VPM and Tf-CVPM as shown in

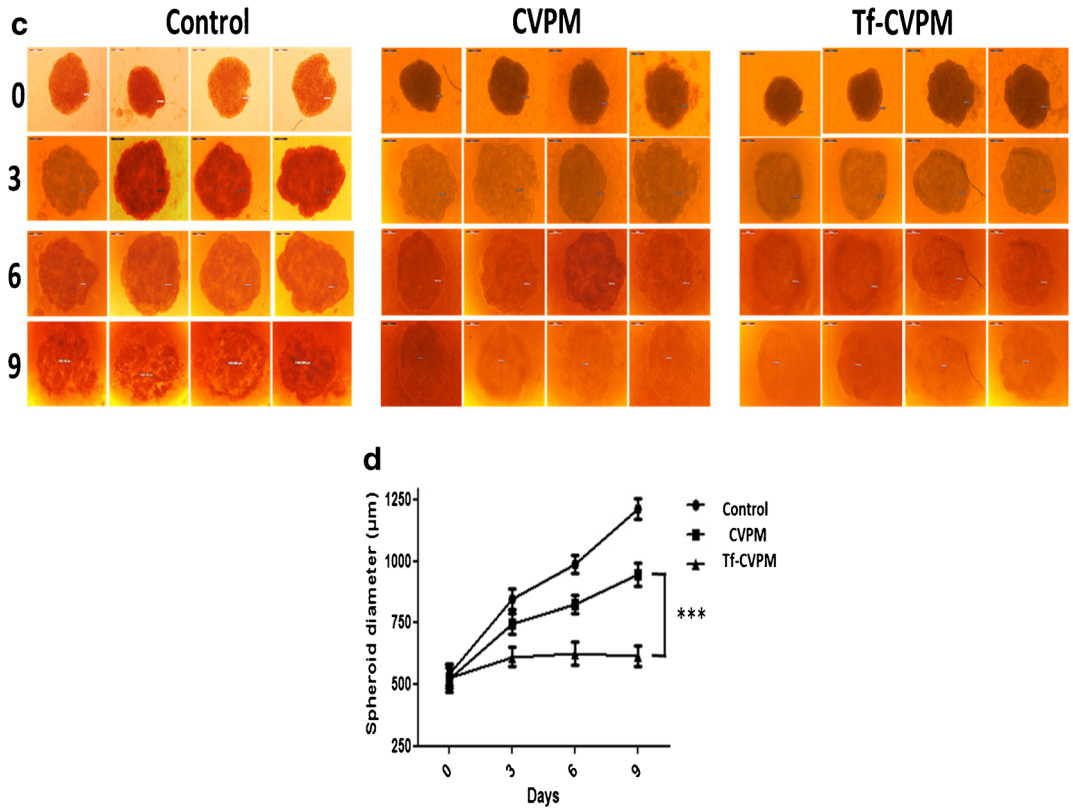

Fig. 5 (continued)

Fig. 4. This is obvious as α-tocopherol and α-tocopherol-conjugated polymers exert apoptosis-inducing, anti-proliferative, and metastasis and multi-drug resistance-inhibitory potential (5,26,38). CUR exhibits anticancer response by variety of inter-related mechanisms, including regulation of cell cycle induction of apoptosis, and senescence, and curbing the tumor growth by inhibiting angiogenesis (39). The major signaling pathways intervened by CUR included NFκB, MAPK, PI3K/Akt/mTOR, and JAK/STAT. Co-delivery of CUR and vitamin-E via active targeting promoted effective reduction in cell viability for Tf-CVPM as observed at both 6 and 24 h time point studies in both the cell lines. Further, it was observed that higher cytotoxicity was observed after 24 h due to the optimum interaction of the drug loaded micelles to complete the cellular death mechanisms.

Development of three dimensional (3D) spheroids using cancer cells and utilization of this spheroidal cell culture systems as a tool to evaluate anticancer response is an emerging and promising approach (17,28,32,33). Spheroids are tumor mass that grows in 3D architecture, and displays heterogeneity, which lacks in monolayer cell culture systems. One of the major disadvantages of conventional therapy is poor penetration of anticancer drugs into the tumor mass, which could not be reproduced in cancer cells grown in monolayers. 3D spheroidal architecture is a close mimic of tumor mass, and represents a better model to study anticancer response, and penetration behavior compared to cells grown in monolayers (40–42). Tf-CVPM displayed higher association and internalization of CUR in HeLa spheroids due to the Tf receptor mediated active targeting of Tf-CVPM to the cancer cells, which was evidenced by higher geo mean fluorescence of spheroidal cells following Tf-CVPM treatment compared to the treatment with CVPM (Fig. 5a). Tf-CVPM penetrated the spheroidal mass efficiently as CUR-fluorescence was visualized by using confocal microscopy in the focal plane at the depth of 60 µm from the spheroidal surface. The CVPM were not able to penetrate the spheroidal mass resulting in significantly lesser fluorescence in the interior of the spheroids. Overall spheroidal cellular association of CUR-mediated by Tf-CVPM was significantly higher compared to CVPM treatment as measured by flow cytometry after dissociation of spheroidal aggregates into single cell suspension following treatment (Fig. 5b). Further, Tf-CVPM demonstrated significantly higher spheroidal growth inhibition compared to CVPM. CVPM treatment could reduce the spheroidal growth rate significantly compared to untreated control spheroids. However, highest growth inhibitory efficiency was observed with Tf-CVPM (Fig. 5c). This could be due to the efficient internalization mediated by the Tf receptors, and induction of anti-tumor response due to the combined presence of CUR, and α-tocopherol conjugated polymer.

CONCLUSION

Here, tumor homing ligand, transferrin-anchored vitamin-E based self-assembled amphiphilic polymer has been developed for active cancer targeting for the delivery of loaded cargo efficiently to achieve superior anticancer response. The result indicated that Tf was successfully anchored on the surface of the pre-developed PEGylated Vitamin-E/Lipid core micelles. The physico-chemical data indicated the formation of stable micelles, Tf-CVPM with comparable particle size, zeta potential, drug loading and encapsulation efficiencies compared to CVPM. The Tf-VPM could deliver the loaded cargo, CUR efficiently to the Tf-over-expressing cancer cells, HeLa, and HepG2, as indicated by the enhanced association of CUR fluorescence following Tf-CVPM treatment in both the cells, in monolayers and in 3D cultures. The enhanced cellular association of CUR following Tf-CVPM treatment resulted in improved cytotoxic response in both the cell lines compared to CVPM. Tf-CVPM could curb the spheroidal growth efficiently compared to CVPM as determined in spheroidal tumor growth inhibition assay. The newly developed nanomedicine utilized combined presence of CUR and α-TOS-conjugated polymer to elicit synergistic anticancer response, which was enhanced drastically by endowing active cancer targeting potential to the nanocarrier by Tf-anchorage on the surface. The resultant multifunctional nanomedicine has the potential to be utilized in cancer therapy and justifies further exploration for clinical translation.

ACKNOWLEDGMENTS AND DISCLOSURES

The work was supported in part by the grants provided by the Department of Science and Technology (CS-269/2013), Government of India and the Department of Biotechnology (BT/Bio-CARe/07/10003/2013–14), Govt of India to Swati Biswas. Omkara Swami gratefully acknowledges Indian Council of Medical Research (2014–24,190), Department of Health Research, Ministry of Health & Family Welfare, Government of India for awarding him with the Senior Research Fellowship (SRF). There are no conflicts of interest

REFERENCES

1. Muddineti OS, Ghosh B, Biswas S. Current trends in using polymer coated gold nanoparticles for cancer therapy. Int J Pharm. 2015;484(1):252–67.
2. Xin Y, Huang Q, Tang J-Q, Hou X-Y, Zhang P, Zhang LZ, *et al.* Nanoscale drug delivery for targeted chemotherapy. Cancer Lett. 2016;379(1):24–31.
3. Schmitz N, Pfistner B, Sextro M, Sieber M, Carella AM, Haenel M, *et al.* Aggressive conventional chemotherapy compared with high-dose chemotherapy with autologous haemopoietic stem-cell transplantation for relapsed chemosensitive Hodgkin's disease: a randomised trial. Lancet. 2002;359(9323):2065–71.
4. Shi C, Zhang Z, Shi J, Wang F, Luan Y. Co-delivery of docetaxel and chloroquine via PEO–PPO–PCL/TPGS micelles for overcoming multidrug resistance. Int J Pharm. 2015;495(2):932–9.
5. Abdullin TI, Bondar OV, Nikitina II, Bulatov ER, Morozov MV, Hilmutdinov A, *et al.* Effect of size and protein environment on electrochemical properties of gold nanoparticles on carbon electrodes. Bioelectrochemistry. 2009;77(1):37–42.
6. Ford JM, Hait WN. Pharmacology of drugs that alter multidrug resistance in cancer. Pharmacol Rev. 1990;42(3):155–99.
7. te Velde EA, Vogten JM, Gebbink MF, van Gorp JM, Voest EE, Borel Rinkes I. Enhanced antitumour efficacy by combining conventional chemotherapy with angiostatin or endostatin in a liver metastasis model. Br J Surg. 2002;89(10):1302–9.
8. Maeda H, Wu J, Sawa T, Matsumura Y, Hori K. Tumor vascular permeability and the EPR effect in macromolecular therapeutics: a review. J Control Release. 2000;65(1):271–84.
9. Maeda H, Bharate G, Daruwalla J. Polymeric drugs for efficient tumor-targeted drug delivery based on EPR-effect. Eur J Pharm Biopharm. 2009;71(3):409–19.
10. Atta AH, El-Shenawy AI, Refat MS, Elsabawy KM. Preparation and characterization of some gold nanometric compounds with simple organic materials as precursor: spectroscopic, biological and anti-cancer assessments. J Mol Struct. 2013;1039:51–60.
11. Biswas S, Torchilin VP. Nanopreparations for organelle-specific delivery in cancer. Adv Drug Deliv Rev. 2014;66:26–41.
12. Chandrasekharan P, Maity D, Yong CX, Chuang K-H, Ding J, Feng S-S. Vitamin E (d-alpha-tocopheryl-co-poly(ethylene glycol) 1000 succinate) micelles-superparamagnetic iron oxide nanoparticles for enhanced thermotherapy and MRI. Biomaterials. 2011;32(24):5663–72.
13. Kutty RV, Feng S-S. Cetuximab conjugated vitamin E TPGS micelles for targeted delivery of docetaxel for treatment of triple negative breast cancers. Biomaterials. 2013;34(38):10160–71.
14. Muddineti OS, Ghosh B, Biswas S. Current trends in the use of vitamin E-based micellar nanocarriers for anticancer drug delivery. Expert Opin Drug Deliv. 2016;14(6):1–12.
15. Li P-Y, Lai P-S, Hung W-C, Syu W-J. Poly (L-lactide)-vitamin E TPGS nanoparticles enhanced the cytotoxicity of doxorubicin in drug-resistant MCF-7 breast cancer cells. Biomacromolecules. 2010;11(10):2576–82.
16. Hayashi T, Tsai S-Y, Mori T, Fujimoto M, Su T-P. Targeting ligand-operated chaperone sigma-1 receptors in the treatment of neuropsychiatric disorders. Expert Opin Ther Targets. 2011;15(5):557–77.
17. Sriraman SK, Pan J, Sarisozen C, Luther E, Torchilin V. Enhanced cytotoxicity of folic acid-targeted liposomes co-loaded with C6 ceramide and doxorubicin: in vitro evaluation on HeLa, A2780-ADR, and H69-AR cells. Mol Pharm. 2016;13(2):428–37.
18. Zeng X, Sun Y-X, Qu W, Zhang X-Z, Zhuo R-X. Biotinylated transferrin/avidin/biotinylated disulfide containing PEI bioconjugates mediated p53 gene delivery system for tumor targeted transfection. Biomaterials. 2010;31(17):4771–80.
19. Tortorella S, Karagiannis TC. Transferrin receptor-mediated endocytosis: a useful target for cancer therapy. J Membr Biol. 2014;247(4):291–307.
20. Yue J, Liu S, Wang R, Hu X, Xie Z, Huang Y, *et al.* Transferrin-conjugated micelles: enhanced accumulation and antitumor effect for transferrin-receptor-overexpressing cancer models. Mol Pharm. 2012;9(7):1919–31.
21. Abouzeid AH, Patel NR, Sarisozen C, Torchilin VP. Transferrin-targeted polymeric micelles co-loaded with curcumin and paclitaxel: efficient killing of paclitaxel-resistant cancer cells. Pharm Res. 2014;31(8):1938–45.

22. Chen H, Zhang T, Zhou Z, Guan M, Wang J, Liu L, *et al.* Enhanced uptake and cytotoxity of folate-conjugated mitoxantrone-loaded micelles via receptor up-regulation by dexamethasone. Int J Pharm. 2013;448(1):142–9.
23. Nam J-P, Park S-C, Kim T-H, Jang J-Y, Choi C, Jang M-K, *et al.* Encapsulation of paclitaxel into lauric acid-O-carboxymethyl chitosan-transferrin micelles for hydrophobic drug delivery and site-specific targeted delivery. Int J Pharm. 2013;457(1):124–35.
24. Zhang P, Hu L, Yin Q, Zhang Z, Feng L, Li Y. Transferrin-conjugated polyphosphoester hybrid micelle loading paclitaxel for brain-targeting delivery: synthesis, preparation and in vivo evaluation. J Control Release. 2012;159(3):429–34.
25. Muthu MS, Kutty RV, Luo Z, Xie J, Feng S-S. Theranostic vitamin E TPGS micelles of transferrin conjugation for targeted co-delivery of docetaxel and ultra bright gold nanoclusters. Biomaterials. 2015;39:234–48.
26. Muddineti OS, Kumari P, Ghosh B, Torchilin VP, Biswas S. d-α-Tocopheryl succinate/Phosphatidyl ethanolamine conjugated amphiphilic polymer-based Nanomicellar system for the efficient delivery of curcumin and to overcome multiple drug resistance in cancer. ACS Appl Mater Interfaces. 2017;9:16778–92.
27. Torchilin V. Targeted polymeric micelles for delivery of poorly soluble drugs. Cell Mol Life Sci. 2004;61(19):2549–59.
28. Sarisozen C, Abouzeid AH, Torchilin VP. The effect of co-delivery of paclitaxel and curcumin by transferrin-targeted PEG-PE-based mixed micelles on resistant ovarian cancer in 3-D spheroids and in vivo tumors. Eur J Pharm Biopharm. 2014;88(2):539–50.
29. Wu H, Zhu L, Torchilin VP. pH-sensitive poly (histidine)-PEG/DSPE-PEG co-polymer micelles for cytosolic drug delivery. Biomaterials. 2013;34(4):1213–22.
30. Yang C, Chen H, Zhao J, Pang X, Xi Y, Zhai G. Development of a folate-modified curcumin loaded micelle delivery system for cancer targeting. Colloids Surf B: Biointerfaces. 2014;121:206–13.
31. Liang N, Sun S, Li X, Piao H, Piao H, Cui F, *et al.* Alpha-tocopherol succinate-modified chitosan as a micellar delivery system for paclitaxel: preparation, characterization and in vitro/in vivo evaluations. Int J Pharm. 2012;423(2):480–8.
32. Sriraman SK, Salzano G, Sarisozen C, Torchilin V. Anti-cancer activity of doxorubicin-loaded liposomes co-modified with transferrin and folic acid. Eur J Pharm Biopharm. 2016;105:40–9.
33. Pereira PM, Berisha N, Bhupathiraju NDK, Fernandes R, Tomé JP, Drain CM. Cancer cell spheroids are a better screen for the photodynamic efficiency of glycosylated photosensitizers. PLoS One. 2017;12(5):e0177737.
34. Li L, Yang Q, Zhou Z, Zhong J, Huang Y. Doxorubicin-loaded, charge reversible, folate modified HPMA copolymer conjugates for active cancer cell targeting. Biomaterials. 2014;35(19):5171–87.
35. Liu Z, Gao X, Kang T, Jiang M, Miao D, Gu G, *et al.* B6 peptide-modified PEG-PLA nanoparticles for enhanced brain delivery of neuroprotective peptide. Bioconjug Chem. 2013;24(6):997–1007.
36. Harding C, Heuser J, Stahl P. Receptor-mediated endocytosis of transferrin and recycling of the transferrin receptor in rat reticulocytes. J Cell Biol. 1983;97(2):329–39.
37. McMahon HT, Boucrot E. Molecular mechanism and physiological functions of clathrin-mediated endocytosis. Nat Rev Mol Cell Biol. 2011;12(8):517–33.
38. Danhier F, Kouhé TTB, Duhem N, Ucakar B, Staub A, Draoui N, *et al.* Vitamin E-based micelles enhance the anticancer activity of doxorubicin. Int J Pharm. 2014;476(1):9–15.
39. Tima S, Ampasavate SCA, Berkland C, Okonogi S. Stable curcumin-loaded polymeric micellar formulation for enhancing cellular uptake and cytotoxicity to FLT3 overexpressing EoL-1 leukemic cells. Eur J Pharm Biopharm. 2017;114:57–68.
40. Zanoni M, Piccinini F, Arienti C, Zamagni A, Santi S, Polico R, *et al.* 3D tumor spheroid models for in vitro therapeutic screening: a systematic approach to enhance the biological relevance of data obtained. Sci Rep. 2016;6:19103.
41. Sambale F, Lavrentieva A, Stahl F, Blume C, Stiesch M, Kasper C, *et al.* Three dimensional spheroid cell culture for nanoparticle safety testing. J Biotechnol. 2015;205:120–9.
42. Perche F, Torchilin VP. Cancer cell spheroids as a model to evaluate chemotherapy protocols. Cancer Biol Ther. 2012;13(12):1205–13.